

# Dynamic control of Bessel beams with longitudinally varying polarization through liquid-crystal anisotropic axicons

María del Mar Sánchez-López<sup>\*a,b</sup>, Ignacio Moreno<sup>a,c</sup>, Tomasz Jankowski<sup>d</sup>, Noureddine Bennis<sup>d</sup>, Anna Spadlo<sup>d</sup>, José Francisco Algorri<sup>e,f</sup>

<sup>a</sup> Instituto de Bioingeniería, Universidad Miguel Hernández de Elche, 03202 Elche, Spain

<sup>b</sup> Departamento de Física Aplicada, Universidad Miguel Hernández de Elche, 03202 Elche, Spain

<sup>c</sup> Departamento de Ciencia de Materiales, Óptica y Tecnología Electrónica, Universidad Miguel Hernández de Elche, 03202 Elche, Spain

<sup>d</sup> Institute of Applied Physics, Military University of Technology, 00908 Warsaw, Poland

<sup>e</sup> Photonics Engineering Group, University of Cantabria, Santander, 39005, Spain

<sup>f</sup> CIBER de Bioingeniería, Biomateriales y Nanomedicina, Instituto de Salud Carlos III, 28029 Madrid, Spain

## ABSTRACT

In this work we discuss liquid-crystal (LC) anisotropic axicons for the dynamic control of the Bessel beam polarization variation along propagation. We first present a technique that employs a LC spatial light modulator (LC-SLM) to display two diffractive axicons, each one affecting one of the two orthogonal linear polarization components. If the two axicons have a slightly different period, a periodic variation in the polarization state of the Bessel beam occurs over propagation. Second, we present a more compact alternative consisting in a combination of a refractive axicon and a LC element of linear phase profile along the radial coordinate. This combination creates a compound compact and tunable anisotropic axicon that produces Bessel beams with tunable polarization modulation. The capability of changing the polarization state of the Bessel beam along its propagation opens new venues in axial polarimetry, optical trapping in multiple planes or axial-dependent laser microfabrication.

**Keywords:** Anisotropic axicon, Polarization control, Bessel beams, liquid-crystal axicon, spatial light modulators.

## 1. INTRODUCTION

Because of their unique line-focusing and non-diffracting properties, Bessel beams [1,2] find applications in materials processing, optical trapping and free-space optical communications [3]. The most efficient way to generate a Bessel beam is through an axicon, also known as a conical lens. Refractive axicons are commercially available but their performance parameters (clear aperture and deflection angle) cannot be tuned. Instead, tunable diffractive axicons based on liquid-crystal technology make use of the optical phase modulation characteristic of liquid crystals. Programmable axicons have been demonstrated using liquid-crystal spatial light modulators (SLM) [4], or with other liquid-crystal (LC) components [5,6]. All these systems generate tunable Bessel beams, with a uniform state of polarization.

In general, Bessel beams present intensity variations along the depth of focus (DOF) distance and methods have been developed [7] to correct for these effects and engineer the axial intensity profile, typically to achieve a flat response, in what is known as an optical needle. Here we focus on a different type of engineering Bessel beams, consisting in modifying the state of polarization (SOP) along propagation. We first review a technique based on using a SLM to display two different diffractive axicons, each one affecting one of the two orthogonal linear polarization components and having a different period [8]. The combination of such axicons with spiral phases led to higher-order vector Bessel beams with periodically varying polarization along propagation [9]. Such SOP oscillatory behavior was further demonstrated with other SLM-based optical systems [10-12]. Metasurfaces offer a more compact and efficient alternative to produce axicons by creating artificial birefringent spatial microstructures [13], where arbitrary polarization functions that vary along the optical path of the beam have been demonstrated [14]. However, these optical elements are not tunable. LC components

---

\* [mar.sanchez@umh.es](mailto:mar.sanchez@umh.es), phone: (+34) 966658329; web: <http://tecnopto.edu.umh.es/>

exhibit natural birefringence and represent an alternative and well-established technology [15] to build such tunable axicon devices.

Thus, in the second part of the work we present a compact tunable anisotropic axicon that yields the results presented in [8] by combining a LC axicon with a refractive axicon. While the refractive axicon equally deviates all polarization states, the LC element only adds or subtracts a conical phase to the polarization component parallel to the extraordinary refractive index. Therefore, an anisotropic axicon is effectively built that creates a polarized Bessel beam exhibiting a SOP with tunable variation along propagation [16].

## 2. ANISOTROPIC AXICON IN A SLM-BASED OPTICAL SYSTEM

Figure 1 shows the experimental setup built at San Diego State University and first developed in [17]. The system is useful to encode two independent phase patterns on two orthogonal linear polarization states of an input laser beam. The key element is a parallel-aligned transmissive LC-SLM from Seiko-Epson, with  $640 \times 480$  pixels of pixel size  $\Delta = 42 \mu\text{m}$ . This device spatially modulates the phase of the linear polarization component parallel to the LC director, in this case the vertical component in the laboratory framework. On the contrary, the polarization component perpendicular to the LC director acquires a constant phase. The system in Fig. 1 allows the independent modulation of both polarization components by passing the beam twice through the SLM and dividing its screen in two halves where a different phase mask is addressed.

The input beam from an argon ion laser is spatially filtered and collimated with lens L1. Then, it is linearly polarized at  $45^\circ$  with respect to the SLM LC director. It illuminates the left part of the SLM screen, where the phase pattern named A is displayed. This phase pattern is encoded in the vertical polarization component, while the horizontal polarization component remains unaffected. After the SLM, a 4f system in reflection is built with lens L2 and a mirror, by placing the lens a distance equal to its focal length ( $f_2$ ) from the SLM, and the mirror also a distance  $f_2$  behind the lens. This makes the beam return to the SLM as an image of unit magnification. A quarter-wave plate (QWP) located before the lens is oriented at  $45^\circ$ , so the double pass of the beam provokes a switch of the vertical and horizontal polarization components when the beam returns back to the right part of the SLM screen. The phase pattern named B, which is addressed in the right part of the SLM, is therefore encoded in the polarization component that was not affected in the first pass through the SLM. This way, the phase patterns (A and B) are encoded respectively in the horizontal and vertical polarization components of the final output beam.

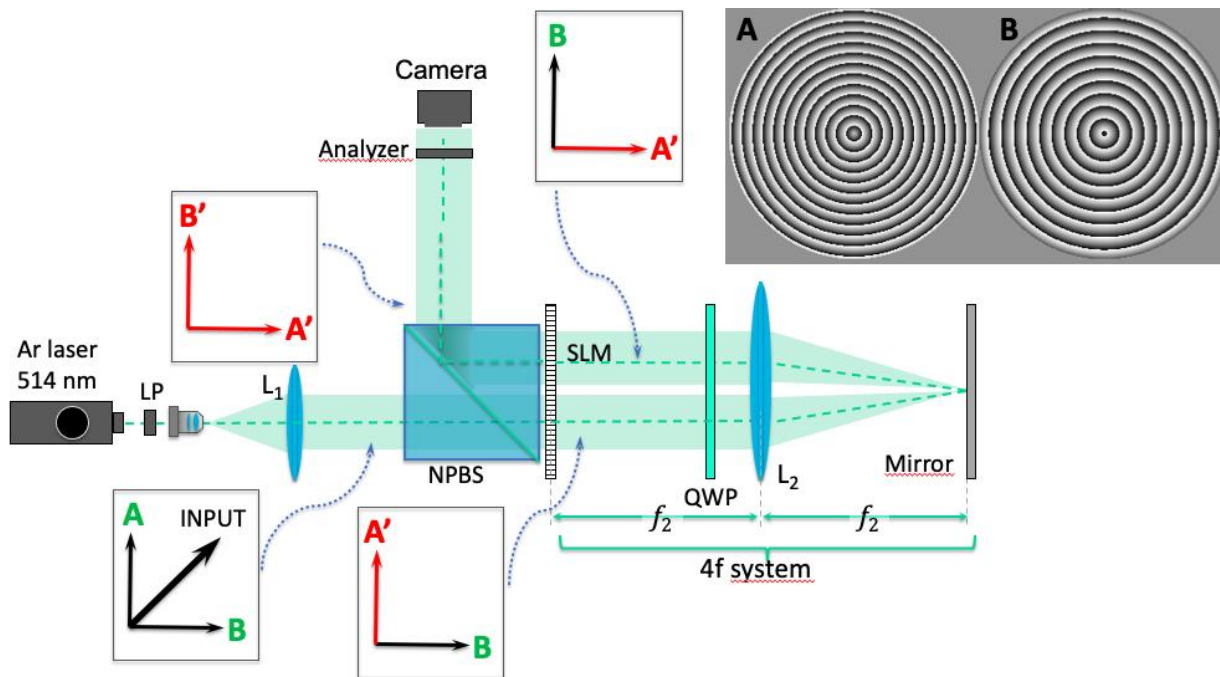


Figure 1. Scheme of the experimental system to encode two independent phase patterns (A and B) on two orthogonal polarization components. The inset shows the image addressed to the SLM to generate an anisotropic axicon.

In this work we are interested in producing anisotropic axicons. The inset shown on the top right part of Fig. 1 illustrates the gray level pattern that must be displayed on the SLM to generate such element. Each half of the SLM screen encodes a diffractive axicon, i.e., a phase mask where the phase grows linearly with the radial coordinate  $r = \sqrt{x^2 + y^2}$  as:

$$g(r) = \exp \left[ -i \left( \frac{2\pi r}{p} \right)_{\text{mod} 2\pi} \right], \quad (1)$$

where  $p$  denotes the period of the diffractive axicon. Such an axicon generates a Bessel beam  $e^{ik_z z} J_0(k_r r)$  with radial wavenumber given by

$$k_r = \frac{2\pi}{p} = k \sin(\theta), \quad (2)$$

where  $\theta$  is the deflected angle given by the diffraction grating equation  $\lambda/p = \sin(\theta)$  and  $k = 2\pi/\lambda$  is the wavenumber [7,16]. The Bessel beam propagation constant is defined by the axial wavenumber:

$$k_z = \sqrt{k^2 - k_r^2} = k \cos(\theta), \quad (3)$$

Therefore, an anisotropic axicon is generated by using two diffractive axicon masks in A and B with different periods  $p_H$  and  $p_V$  respectively. This makes the Bessel beam propagation constants be different in the vertical and horizontal polarizations, so there is an axial phase shift  $\Phi(z)$  between the two components of the Bessel beam given by:

$$\Phi(z) = \phi_V - \phi_H = k_{zV} z - k_{zH} z = (k_{zV} - k_{zH}) z, \quad (4)$$

where  $k_{zV}$  and  $k_{zH}$  are the axial wavenumbers encoded in the vertical and horizontal polarization components. We define as  $Z$  the axial distance for which the phase  $\Phi(z)$  varies by  $2\pi$ , i.e.:

$$Z = \frac{2\pi}{k_{zV} - k_{zH}} = \frac{\lambda}{\cos(\theta_V) - \cos(\theta_H)} \cong \frac{2}{\lambda} \left( \frac{p_V^2 p_H^2}{p_V^2 - p_H^2} \right), \quad (5)$$

where  $\theta_V$  and  $\theta_H$  are the deflection angles, and  $p_V$  and  $p_H$  are the axicon periods for the vertical and horizontal polarization components respectively, and where the small angle approximation as well as the diffraction grating's equation is applied in the last step to retrieve  $\cos(\theta) \cong 1 - \frac{1}{2}\theta^2 = 1 - \frac{1}{2}(\lambda/p)^2$ .

Figure 2 illustrates the experimental results obtained with the system in Fig. 1. Here the diffractive axicon encoded in the vertical polarization has a period  $p_V = 5$  pixels, while the one encoded in the horizontal polarization is selected with a period of  $p_H = 4.615$  pixels (i.e. it is an asynchronous axicon, where the phase values are not repeated in each period [18]). These values are selected so 13 periods  $p_H$  fit within 60 pixels, while for  $p_V$  only 12 periods fit [8]. Thus, for the SLM pixel size ( $\Delta = 42 \mu\text{m}$ ), the phase shift  $\Phi(z)$  in Eq. (4) changes by  $2\pi$  every distance  $Z = 1$  m. This implies that the polarization variation of the Bessel beam along the  $z$  propagation axis is repeated periodically every one-meter, performing a complete circle on the Poincaré sphere along the meridian in the S2-S3 plane. Namely, starting from the linear polarization oriented at  $45^\circ$ , it becomes right circularly polarized (RCP), then linearly polarized oriented at  $135^\circ$ , left circularly polarized (LCP) and finally back to a linear state oriented at  $45^\circ$ , and this is repeated every distance  $Z = 1$  m.

The experimental results in Fig. 2 confirm these polarization transformations. The first row in Fig. 2 shows the experimental intensity pattern captured at a close distance from the beam-splitter output, that we denote as  $z = z_0$ . The image indicated as "NoA" corresponds to the case without analyzer. It shows the characteristic Bessel beam pattern. We added a bias phase to one of the axicon patterns in order to make the center of the beam in this plane linearly polarized, with orientation at  $+45^\circ$ . This is verified by analyzing the Bessel beam in this plane with a linear polarizer oriented at zero,  $45^\circ$ ,  $90^\circ$  and  $135^\circ$ , as well as with LCP and RCP circular polarizers. This is shown in the first row in Fig. 2. It is observed that the Bessel beam appears bright when the linear analyzer is oriented at  $+45^\circ$ , while it appears dark when the linear analyzer is oriented at  $135^\circ$ . As expected, the intensity is approximately one half when the linear analyzer is horizontally or vertically oriented, as well as for left (LCP) and right (RCP) circular analyzers.

Then, we experimentally verified the changes of the SOP along the propagation axis. In order to capture the corresponding intensity patterns at precise distances, and avoid any possible misalignment when moving the camera, we applied a technique that performs the virtual propagation of the beam using a fast Fresnel propagation algorithm [19]. This enabled us to evaluate the beam propagation without moving either the SLM nor the camera. The algorithm was applied to

propagation distances  $Z/4$ ,  $Z/2$  and  $3Z/4$ . The corresponding results are presented in the second, third and fourth rows in Fig. 2. The results without analyzer (left column) show the nondiffracting characteristic propagation of the Bessel beam. However, there is a continuous linear change of the SOP, which becomes clear when the polarization analyzers are placed before the camera. For a propagation of  $Z/4$ , the  $\pi/2$  retardance variation makes the center of the beam LCP polarized. This is verified as the intensity at the center of the beam remains constant when rotating the linear polarizer, whilst it appears bright and dark when the left and right circular analyzers are employed. The results on the third and fourth rows, corresponding to propagation distances  $Z/2$  and  $3Z/4$ , demonstrate that the beam is linearly polarized at  $-45^\circ$  and RCP polarized at these two planes respectively. Therefore, these results verify the linear change in the SOP of the Bessel beam generated by this conical retarder axicon system. Likewise, a vortex diffractive anisotropic axicon was obtained by adding a spiral phase to the axicon phase, thus generating a scalar higher-order Bessel beam with longitudinally varying SOP [8].

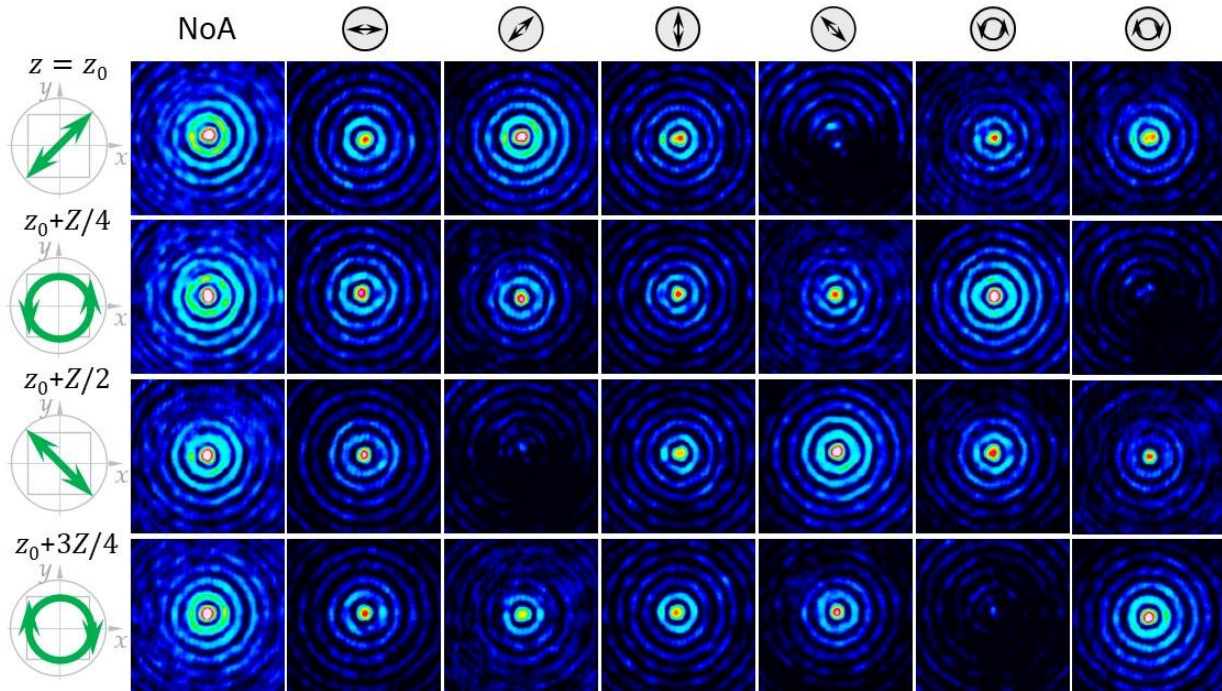


Figure 2. Experimental results at four axial distances separated by  $Z/4$ . Images are captured without analyzer (NoA) and with linear analyzers oriented at zero,  $45^\circ$ ,  $90^\circ$ ,  $135^\circ$ , and with LCP and RCP analyzers. The different applied analyzers are indicated on the top.

### 3. COMPACT ANISOTROPIC LIQUID-CRYSTAL AXICON

The results in the previous section demonstrate the realization of the Bessel beam with continuous polarization transformation upon propagation. However, it requires the bulk system in Fig 1, which introduces severe losses due to the use of the beam splitter and the SLM. Other architectures relying on two SLMs that independently modulate the two orthogonal polarization components, like in [20] are also bulky optical setups that require careful alignment. We recently demonstrated an alternative compact and efficient way of generating a Bessel beam with longitudinally-varying polarization by using a LC tunable axicon cascaded with a refractive axicon [16]. The LC axicon was fabricated with a transmission-electrode technique to achieve a controllable radial wavenumber. The refractive axicon equally deviates all polarization states. Therefore, when combining both elements, the LC axicon adds a radial phase only to the polarization component parallel to the LC director axis. As a consequence, two orthogonally polarized Bessel beams with different inclination are generated, thus exhibiting a phase-shift along propagation. We use a refractive axicon of much higher power than the LC axicon; therefore, the Bessel beam depth of focus is basically determined by the refractive element, while the LC axicon controls the SOP modulation along propagation.

The LC device structure is simple, can be fabricated in one lithographic step, and only requires two voltage sources. It consists of an ITO electrode that produces a high resistance through a high aspect ratio design. Therefore, the current is low, but the voltage is continuous along the electrode. Then, this voltage is homogeneously distributed by a set of floating

concentric electrodes across the active area. The structured used is the one in [21]. After the patterning process to achieve the transmission electrode on ITO coated glass, a polyimide alignment layer is spin-coated on the patterned substrates. This layer is rubbed to obtain a molecular homogeneous alignment. Following the rubbing treatment, the LC axicon device was assembled. A LC mixture having positive dielectric anisotropy and high birefringence [22] was infiltrated into the cavity.

In Fig. 3 the LC device is viewed between parallel polarizers oriented at  $45^\circ$  relative to the LC director. This way, the LC retardance  $\phi$  can be visualized as intensity variations. Figures 3(a), 3(b) and 3(c) show three examples for different  $V_{rms}$  voltages applied to the device. Specifically, the same fixed voltage ( $0.5 V_{rms}$ ) is set at the axicon center whereas a different higher voltage ( $2.5, 3.0$  and  $3.5 V_{rms}$ ) is applied at the axicon perimeter, through the concentric electrodes. Well-contrasted interference rings are visible within a circular central active area of radius  $r_{max} = 5 mm$ , showing how the LC retardance varies along the radial coordinate as  $I(r) = \cos^2[\phi(r)/2]$ . Below each image, the inset shows the intensity profile along a diameter in the central LC aperture. The separation between fringes appears approximately constant. As the applied  $V_{rms}$  increases, the number of interference rings decreases. In each case, the retardance  $\phi(r)$  is retrieved from the interference patterns and shown in Fig. 3(d). The experimental phase profile  $\phi(r)$  approximates rather well a linear radial phase variation in all three cases, as required for an axicon. Note that the axicon profile only affects the polarization component parallel to the LC director axis (here, vertically aligned), for which it induces very small radial wavenumber  $k_r^{LC}$ , thus leading to a very small deflection angle.

To achieve higher deflection powers and obtain an anisotropic compound axicon, we combine the previous LC axicon with a refractive glass axicon. The refractive axicon is a commercial component (Thorlabs, model AX252-A) made of UV fused silica, with a clear aperture of 25 mm and a deflection angle of 0.9 degrees (one order of magnitude greater than those obtained with the LC axicon). Therefore, in this case the radial wavenumbers for the horizontal and vertical polarization components are  $k_{rH} = k_r^R$  and  $k_{rV} = k_r^R + k_r^{LC}$  where  $k_r^R$  stands for the radial wavenumber induced by the refractive axicon, which affects both polarization components. Their difference yields the retardance given in Eq. (4), thus providing the polarization transformation of the Bessel beam upon its propagation.

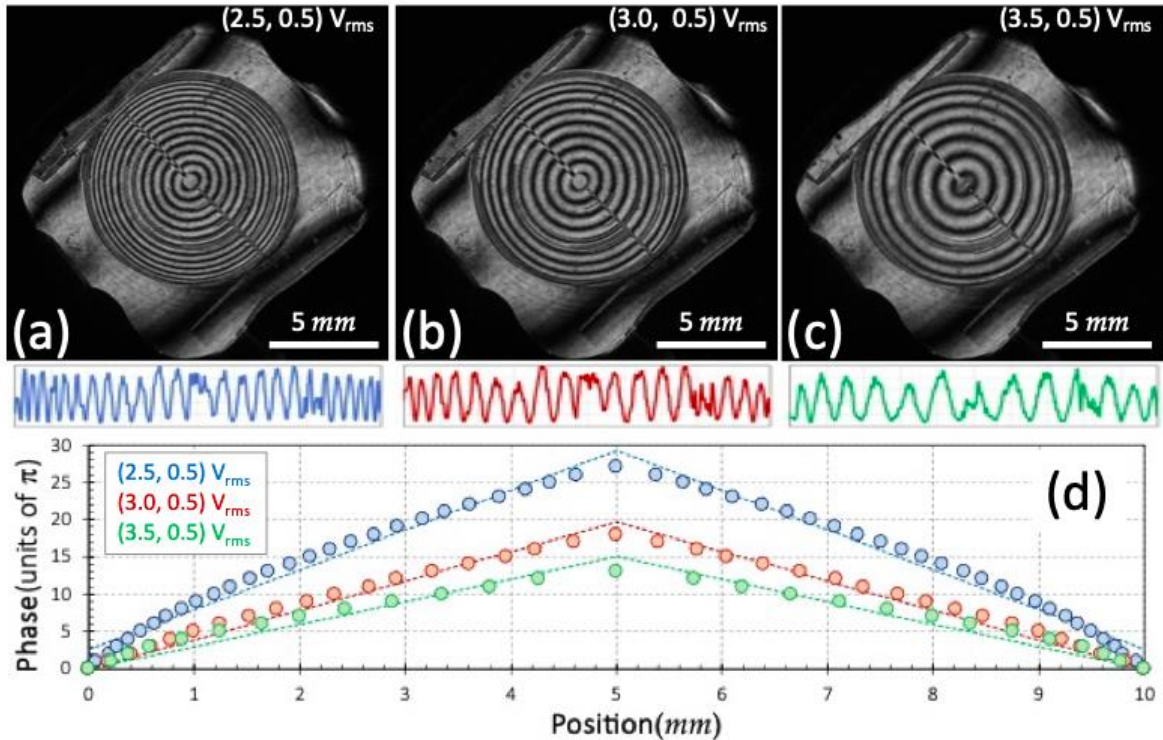


Figure 3. (a)-(c) Captures of the interference pattern for different voltages addressed to the LC axicon (the insets show the intensity profile along a diameter in the central active area). (d) Retrieved phase profile along the horizontal direction and its best linear fit.

Taking into account the slope of the phase profiles shown in Fig. 3(d), axial periods  $Z$  of 23 mm, 31 mm and 42 mm are expected for the applied voltages (2.5, 0.5), (3.0, 0.5) and (3.5, 0.5)  $V_{\text{rms}}$  respectively. Figure 4 shows the intensity of the Bessel beam center as a function of the propagation distance between 75 and 200 mm, when the compound axicon is illuminated with a He-Ne laser beam of 633 nm wavelength, linearly polarized at  $45^\circ$ , and a circular polarizer analyzer is placed before the camera detector. The curves confirm the expected oscillatory behaviour, showing a faster oscillation for the applied voltage (2.5, 0.5)  $V_{\text{rms}}$  and featuring wider oscillations for higher voltages. The arrows in Fig. 4 indicate the expected spatial periods for the three cases, which match quite well the experiments.

For each pair of addressed voltages, measurements were repeated using different polarization analyzers in front of the camera in order to measure the Stokes parameters [16] and represent the polarization state (SOP) in the Poincaré sphere (PS). Figure 5(a) represents the expected SOP variation. Since the input light is linearly polarized at  $45^\circ$ , its location on the PS is on the positive  $S_2$  axis (indicated as input SOP in Fig. 5(a)). The anisotropic axicon creates a linear retardance  $\Phi(z)$  between the horizontal and vertical polarization components which ideally produces a Bessel beam SOP trajectory in the PS along the meridian in the  $S_2-S_3$  plane (plane  $S_1 = 0$ ). The circle is completed every period of oscillation over the distance  $Z$ . Figure 5(b) shows that the experimental trajectory retrieved from the experimental data corresponding to the voltage pair (3.0, 0.5)  $V_{\text{rms}}$ . These results confirm that the experimental points all locate approximately on the  $S_2 - S_3$  plane, bearing a good agreement with theory.

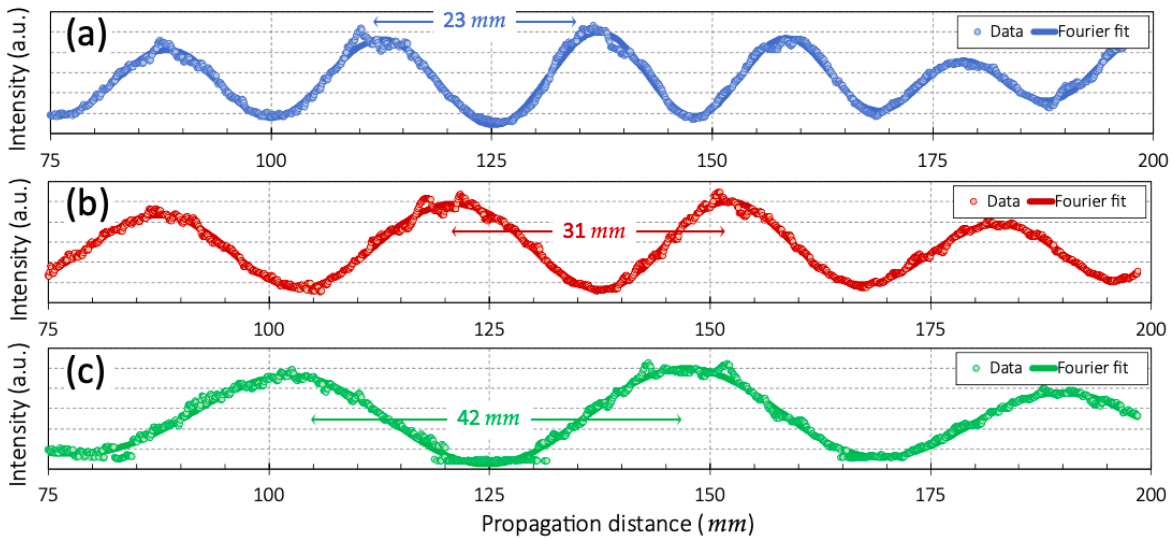


Figure 4. Intensity along the propagation distance with the LC axicon tuned with (a) (2.5, 0.5)  $V_{\text{rms}}$ , (b) (3.0, 0.5)  $V_{\text{rms}}$  and (c) (3.5, 0.5)  $V_{\text{rms}}$ . The arrows indicate the expected periods for the three cases.

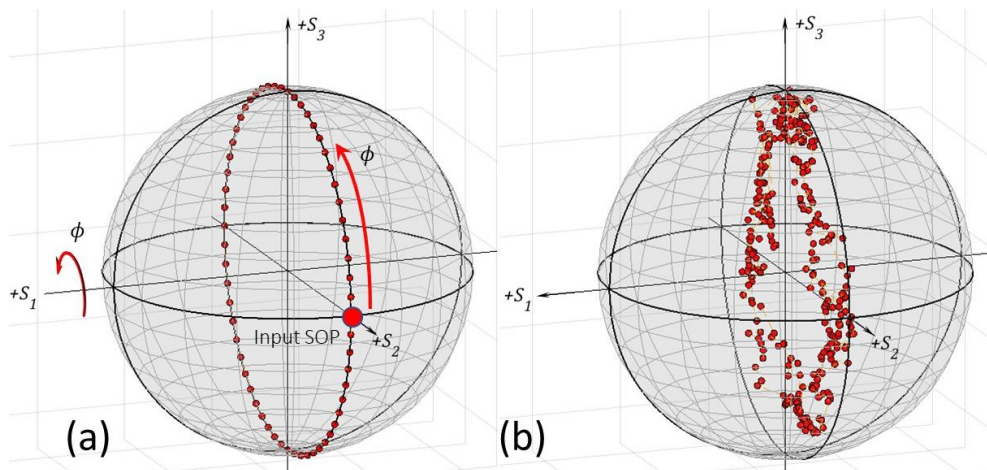


Figure 5. (a) Ideal theoretical SOP trajectory in the Poincaré sphere along the Bessel beam propagation. (b) Experimental SOP trajectory derived from the data corresponding to (3.0, 0.5)  $V_{\text{rms}}$ .

## 4. CONCLUSIONS

In summary, we have presented two methods to generate an anisotropic axicon that produces a Bessel beam with continuous periodic polarization transformation upon propagation. Both methods rely on having different propagation constants in the two orthogonal polarization components of the Bessel beam, such that there is an axial phase shift between these components. The first system is based on a parallel-aligned LC-SLM, where the light beam passes twice through the SLM and modulates one of the two orthogonal polarization components in each pass. Dividing the SLM screen in two halves and addressing two diffractive axicons with slightly different periods creates the diffractive anisotropic axicon [8]. The technique is extremely versatile, since other phase functions can be added to the two axicon phases. Thus, by adding a spiral phase of opposite charge to each axicon phase pattern we can generate a vector Bessel beam where the polarization state changes from being radially polarized to being slanted, then it becomes azimuthally polarized, opposite slanted and again radially polarized [9]. However, the optical setup is bulky and requires fine alignment.

The second method is a compound axicon that combines a regular refractive axicon with a LC tunable axicon [16]. The latter only affects the polarization component parallel to the LC director. This tunable LC axicon was fabricated using the transmission-electrode technique [21], so its phase profile can be tuned by applying different  $V_{\text{rms}}$  values, therefore changing the spatial period of the polarization oscillation in the Bessel beam. This compound axicon is a very compact and much efficient way of generating Bessel beams with tunable polarization modulation. Cascading it with a spiral phase plate it will generate scalar higher-order Bessel beams, whilst cascading it with a q-plate will generate vector Bessel beams as described above, where the SOP describes a trajectory around the equator of the higher-order Poincaré sphere [23].

The tunable longitudinal polarization control of Bessel beams achieved with these approaches could find applications in materials processing or optical traps, requiring the polarization modulation of the non-diffracting beam, optical trapping in multiple planes or in axial polarimetry.

## ACKNOWLEDGEMENTS

We acknowledge financial support by Ministerio de Ciencia e Innovación, Spain (ref.: PID2021-126509OB-C22) and Generalitat Valenciana (ref. CIAICO/2021/276).

## REFERENCES

- [1] J. Durnin, "Exact solutions for nondiffracting beams. I. The scalar theory", *J. Opt. Soc. Am. A* 4(4), 651-654 (1987).
- [2] J. Durnin, J. J. Miceli, Jr. and J. H. Eberly, "Diffraction free beams", *Phys. Rev. Lett.* 58, 1499-1501 (1987).
- [3] D. McGloin and K. Dholakia, "Bessel beams: diffraction in a new light", *Contemp. Phys.* 46(1), 15-28 (2005).
- [4] J. A. Davis, J. Guertin and D. M. Cottrell, "Diffraction-free beams generated with programmable spatial light modulators", *Appl. Opt.* 32(31), 6368-6370 (1993).
- [5] J. F. Algorri, V. Urruchi, N. Bennis and J. M. Sánchez-Pena, "Modal liquid crystal micro-axicon array", *Opt. Lett.* 39(12), 3476-3479 (2014).
- [6] J. Pereiro-García, M. García-de-Blas, M. A. Geday, X. Quintana and M. Caño-García, "Flat variable liquid crystal diffractive spiral axicon enabling perfect vortex beams generation", *Sci. Rep.* 13, 2385 (2023).
- [7] T. Čižmár and K. Dholakia. "Tunable Bessel light modes: engineering the axial propagation", *Opt. Express* 17(18), 15558-15570 (2009).
- [8] I. Moreno, J. A. Davis, M. M. Sánchez-López, K. Badham and D. M. Cottrell, "Nondiffracting Bessel beams with polarization state that varies with propagation distance," *Opt. Lett.* 40(23), 5451-5454 (2015).
- [9] J. A. Davis, I. Moreno K. Badham, M. M. Sánchez-López and D. M. Cottrell, "Nondiffracting vector beams where the charge and the polarization state vary with propagation distance", *Opt. Lett.* 41(10), 2270-2273 (2016).
- [10] P. Li, Y. Zhang, S. Liu, L. Han, H. Cheng, F. Yu and J. Zhao, "Quasi-Bessel beams with longitudinally varying polarization state generated by employing spectrum engineering", *Opt. Lett.* 41(20), 4811-4814 (2016).
- [11] P. Li, D. Wu, Y. Zhang, S. Liu, Y. Li, S. Qui and J. Zhao, "Polarization oscillating beams constructed by copropagating optical frozen waves", *Photonics Res.* 6(7), 756-760 (2018).
- [12] W.-Y. Wang, J.-X. Guo, S. Liu, J.-Q. Lü and Z.-W. Lu, "Manipulating the variation of polarization during propagation along arbitrary circular trajectory of the Poincaré sphere", *Appl. Phys. Lett.* 121, 161102 (2022).

- [13] W. T. Chen, M. Khorasaninejad, A. Y. Zhu, J. Oh, R. C. Devlin, A. Zaidi and F. Capasso, “Generation of wavelength-independent subwavelength Bessel beams using metasurfaces”, *Light: Sci. & Appl.* 6(5), e16259 (2017).
- [14] A. H. Dorrah, N. A. Rubin, A. Zaidi, M. Tamagnone and F. Capasso, “Metasurface optics for on-demand polarization transformations along the optical path”, *Nat. Photonics* 15, 287–296 (2021).
- [15] J. Beeckman, K. Neyts and P. J. M. Vanbrabant, “Liquid-crystal photonic applications”, *Opt. Eng.* 50(8), 081202 (2011).
- [16] T. Jankowski, N. Bennis, A. Spadlo, J. F. Algorri, M. M. Sánchez-López and I. Moreno, “Liquid crystal anisotropic axicon for the generation of non-diffracting Bessel beams with longitudinally varying polarization”, *Opt. Laser Technol.* 170, 110255 (2024).
- [17] I. Moreno, J. A. Davis, T. M. Hernandez, D. M. Cottrell and D. Sand, “Complete polarization control of light from a liquid crystal spatial light modulator”, *Opt. Express* 20(1), 364–376 (2012).
- [18] J. A. Davis, J. Adachi, D. M. Cottrell, “Diffraction efficiency of nonsynchronously sampled diffraction gratings”, *Opt. Eng.* 41(11), 2983–2986 (2002).
- [19] J. A. Davis, I. Moreno, D. M. Cottrell, C. A. Berg, C. L. Freeman, A. Carmona and W. Debenham, “Experimental implementation of a virtual optical beam propagator system based on a Fresnel diffraction algorithm”, *Opt. Eng.* 54, 103101 (2015).
- [20] P. García-Martínez, D. Marco, J. L. Martínez-Fuentes, M. M. Sánchez-López and I. Moreno, “Efficient on-axis SLM engineering of optical vector modes”, *Opt. Lasers Eng.* 125, 105859 (2020).
- [21] N. Bennis, T. Jankowski, P. Morawiak, A. Spadlo, D. C. Zografopoulos, J. M. Sánchez-Pena, J. M. López-Higuera and J. F. Algorri, “Aspherical liquid crystal lenses based on a variable transmission electrode”, *Opt. Express* 30, 12237–12247 (2022).
- [22] N. Bennis, T. Jankowski, O. Strzeczysz, A. Pakuła, D. C. Zografopoulos, P. Perkowski, J. M. Sánchez-Pena, J. M. López-Higuera and J. F. Algorri, “A high birefringence liquid crystal for lenses with large aperture”, *Sci. Rep.* 12, 14603 (2022).
- [23] G. Milione, H. I. Sztul, D. A. Nolan and R. R. Alfano, “Higher-order Poincaré sphere, Stokes parameters, and the angular momentum of light,” *Phys. Rev. Lett.* 107(5), 053601 (2011).